JOURNAL OF KUFA–PHYSICS
journal.uokufa.edu.iq/index.php/jkp/index | ISSN: 2077–5830

Stabilizing magnetic order of cobalt-based anisotropic nanoparticles prepared using $NaBH_4$ as a reducing agent

Mohammed H. Abbas[1*] **Hashim Jabbar[2]**

Department of Physics, College of Science, University of Basrah, Iraq

Corresponding Author E-mail: [1]mhmdhasn12345@gmail.com, [2]hashim.jabbar@uobasrah.edu.iq

ARTICLE INF.

Article history:
Received: 14 DEC., 2023
Revised: 29 FEB., 2024
Accepted: 04 MAR., 2024
Available Online: 22 JUN 2024

Keywords:

Ferromagnetic material,
Cobalt NPs,
$NaBH_4$,
Hysteresis loop

ABSTRACT

A one-pot chemical method was used to prepare cobalt nanoparticles (Co NPs) by employing sodium borohydride ($NaBH_4$) as a reducing agent, as well as graphite and activated carbon as stabilizer materials. The resulting NPs were characterized by XRD, FE-SEM, EDX mapping and VSM measurements before and after annealing under a mixture of argon and hydrogen atmosphere at 600 ℃, in order to study their structural, morphological, and magnetic properties. This study focused on the shape and size of Co NPs, involving the formation of Co and Co_3O_4 phases with the effect of oxygen as the main factor that can significantly contribute to the magnetic anisotropy. Co NPs exhibited a high saturation magnetization (M_s) value after performing the annealing process, achieving M_s> 99 emu/g when using the graphite stabilizer. The results indicate that surface atoms play a significant role in the modification of magnetic characteristics of Co NPs.

DOI: https://doi.org/10.31257/2018/JKP/2024/v16.i01.14497

استقرار الترتيب المغناطيسي في جسيمات الكوبالت النانوية متباينة الخواص والمحضرة باستخدام $NaBH_4$ كعامل مختزل

محمد حسن عباس، هاشم محمد جبار

(قسم الفيزياء، كلية العلوم، جامعة البصرة، العراق)

الكلمات المفتاحية:

المواد الفيرومغناطيسية،
جسيمات الكوبالت النانوية،
بوروهيدريد الصوديوم،
حلقة الهسترة

الـــخُـــلاصـــة

تم استخدام طريقة كيميائية ذات وعاء واحد لتحضير جسيمات الكوبالت النانوية (Co NPs) عن طريق استخدام بوروهيدريد الصوديوم ($NaBH_4$) كعامل اختزال، وكذلك الگرافيت والكاربون المنشط كمواد مثبتة. شخصت NPs الناتجة بقياسات XRD و FE-SEM و EDX mapping وقياسات VSM قبل وبعد التلدين تحت خليط من غازات الأرگون والهيدروجين عند 600 درجة مئوية من أجل دراسة خصائصها الهيكلية والمورفولوجية والمغناطيسية. ركزت هذه الدراسة على شكل وحجم Co NPs، بما في ذلك تكوين مراحل Co و Co_3O_4 مع تأثير الأوكسجين كعامل رئيسي يمكن أن يساهم بشكل كبير في تباين الخواص المغناطيسية. أظهرت Co NPs قيمة مغنطة تشبع (M_s) عالية بعد إجراء عملية التلدين ، وتساوي M_s > 99 emu / g عندما استخدام مثبت الگرافيت. تشير النتائج إلى أن ذرات السطح تلعب دوراً مهماً في تعديل الخصائص المغناطيسية لـ Co NPs.

1. INTRODUCTION

Magnetic nanoparticles (NPs) have been used in various fields, ranging from nanomedicine to electromagnetic devices in which the particle size affects the magnetic response [1,2]. Nanotechnology has been established based on the collection of physical properties of materials and their nano-dimensions [3]. It is necessary to control magnetic characteristics for the effective use of NPs in applied technologies, so that controlling the shape, size and the surface atoms of the NPs leads to the tuning of magnetic moments and anisotropy [4]. For instance, the magnetic anisotropy decreases when reducing the size of conventional magnetic materials, and superparamagnetic relaxations take place at the nanoscale level (i.e., a few nanometers). One of the most significant ferromagnetic elements is cobalt (Co), which is available in three different crystal forms: *ε*, *hcp* and *fcc*. In turn, these phases determine magnetic and electric characteristics [5]. Numerous factors such as the size and shape of NPs, magnetic interactions, crystal lattice and its defects, and the methods used to prepare the material are related to magnetic properties of Co NPs [6]. Cobalt is utilized in many different applications, including permanent magnets, optical devices, sensors, magnetic recording media, and information storage [7,8]. Co NPs have physical and chemical characteristics that are interconnected to so-called quantum size effects. Such effects are brought about by a decrease in size, thereby modifying the electron density of states [9]. The concept that the interaction between magnetic atoms and surface atoms strongly affects the magnetic properties is one of the core concepts in the physics of magnetic NPs. The variables such as symmetry breaking and hybridization influence both the atoms inside the particle and the atoms on the surface as a result of their interactions, thus changing magnetic properties of NPs [10]. The various preparation techniques of Co NPs (e.g., physical, chemical, and electrochemical methods) allow for precise control over the size and morphology, making them very effective in terms of magnetic properties. The thermal decomposition, hydrothermal reaction, and polyol processes rely on a common reduction method and involve chemical reactions [11,12]. For the application of Co NPs in high-density and fast recording memory devices, a synthetic technique that offers strict control over many structural properties including average size, size distribution, close packing sequences, and morphology must be taken into consideration. In addition to preventing Co NPs from oxidation and mixing, the capping ingredient can promote stability [13].

Cheng et al. [14] used a combination of organic solvent and surfactant along with sodium borohydride ($NaBH_4$) in order to synthesize Co NPs with controlled sizes in the range of 3.2–171.4 nm using an organic solvent-stabilized method. In this regard, decreasing the glycol/water ratio increased the size and aggregation of Co NPs. In another investigation, Morcos et al. [15] synthesized monodisperse Co NPs with extremely small diameters (< 5 nm) in ionic liquids. The as-synthesized NPs with superparamagnetic behavior possessed *ε*-Co phase, which progressively transformed into stable *hcp*-Co phase at room temperature. Alternatively, carbon encapsulated Co NPs were synthesized using a solvothermal method, leading to the co-existence of *fcc*- and *hcp*-Co phases [16]. These NPs were ferromagnetic in nature, having saturation magnetization (M_s)

and coercivity (H_c) of up to 158 emu/g and 206 Oe, respectively.

This paper aims to investigate the reduction of cobalt ions into NPs with and without carbon-based stabilizer materials. Also, $NaBH_4$ is utilized as a strong reducing agent in the synthesis of Co NPs. Various characterization techniques are used to investigate properties of the resulting NPs. This study indicates that carbon can stabilize the structure, morphology, and magnetic properties of oxidized Co NPs.

2. Materials and Methods

2.1. Materials

Cobalt (II) chloride hexahydrate ($CoCl_2.6H_2O$, Merck), $NaBH_4$ (Aldrich, 99%), graphite (Aldrich), carbon (100% activated bulletproof coconut charcoal), and distilled water were used without any further purification.

2.2. Synthesis of Co NPs

A one-pot chemical reduction method was utilized to prepare three samples of Co NPs. For the synthesis of the first sample (S1), 2 g of $CoCl_2.6H_2O$ was dissolved in 100 mL of distilled water under mechanical stirring at 25 ℃. Next, 0.2 M of $NaBH_4$ was drop-wise added to the solution, leading to the reduction of the precursor containing metallic cobalt. The black precipitates then formed during a reaction time of 15 min. In order to prepare the second sample (S2), a stoichiometric amount of $CoCl_2.6H_2O$ was dissolved in 100 mL of distilled water at 25 ℃ for 20 min by using a magnetic stirrer to ensure homogeneity. Afterwards, 0.5 g of graphite was added to the solution. 0.1 M of $NaBH_4$ was also added after 1 h of reaction in order to reduce Co NPs, followed by a rest time of 15 min. The third sample (S3) was prepared using 0.5 g of activated carbon with the same procedure and conditions as described above.

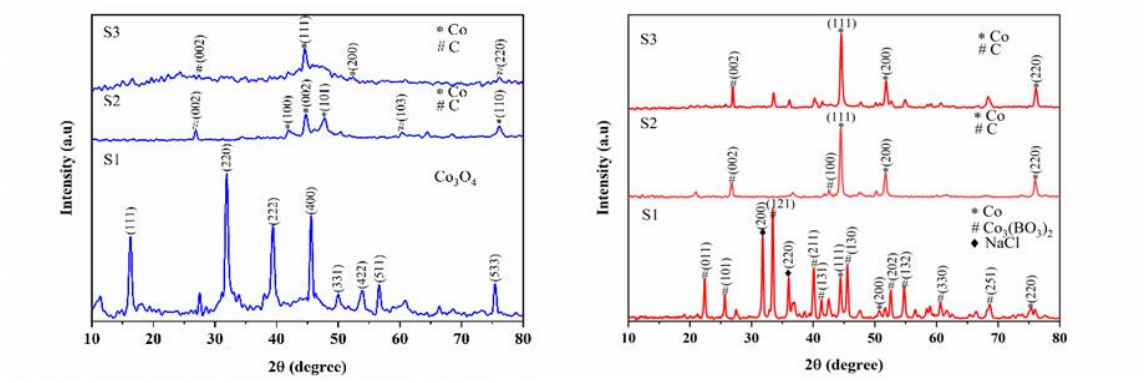

Fig. 1: XRD spectra of Co NP samples (S1, S2, and S3) synthesized by a chemical reduction method before (blue line) and after (red line) annealing.

3. Material Characterizations

X-ray diffraction (XRD) patterns were recorded by a Panalytical X-ray diffractometer (anode source with $CuK\alpha$ radiation, λ = 0.15406 nm, voltage = 40 kV, and current = 30 mA) at 2θ ranging from 10º to 80º. With a scanning speed of 2 min^{-1}, the phase, crystal structure, and crystallite size were determined for powder form of the three samples.

The morphology of Co NPs was investigated using field-emission scanning electron microscopy (FE-SEM, MIRA3 TESCAN). In this case, the average size of the NPs was

determined using particle size distribution histograms generated using data collected from FE-SEM images [17]. The average size was determined using the following formula: $d_n = \sum d_i n_i / \sum n_i$, where n_i is the number of NPs with the selected size range, and d_i is the average diameter of NPs in the selected interval. The energy dispersive X-ray (EDX) analysis was used to determine elemental spectra of the samples. Furthermore, mapping of the spatial distribution of elements in the samples was performed.

By using a vibrating sample magnetometer (VSM, MDK, Iran), room-temperature magnetic characteristics of powder forms of the synthesized samples were precisely measured before and after annealing under an applied magnetic field of up to ± 10 kOe. The quantities commonly used for describing magnetism in materials, including M_s, remanence magnetization (M_r), H_c, and squareness (M_r/M_s) were extracted from hysteresis loops. Within the hysteresis loop, the magnetic field was measured with a relative error of less than 0.0001%.

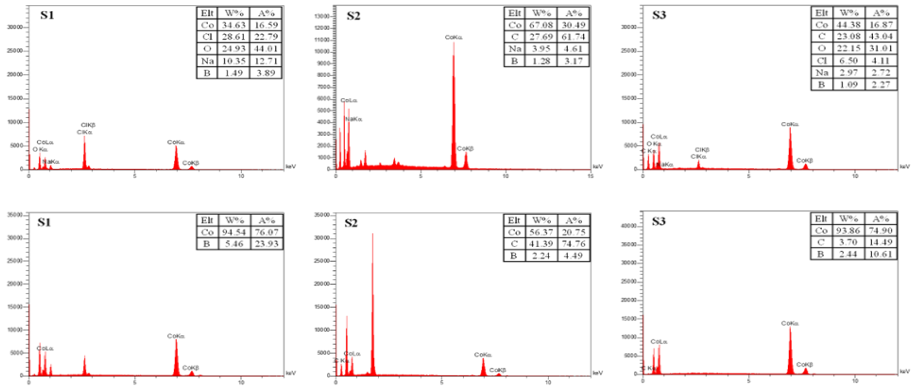

Fig. 2: EDX spectra of Co NP samples before (top panel) and after (bottom panel) annealing.

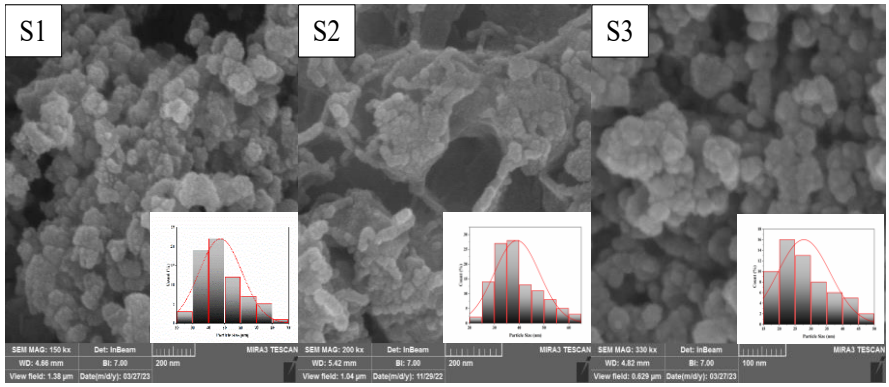

Fig. 3: FE-SEM images of as-synthesized Co NP samples (S1, S2, and S3). The insets represent size distribution histograms with the best fit obtained for Co NPs before annealing.

4. Results and Discussion

Fig. 1 shows XRD patterns of as-synthesized and annealed Co NP samples (S1, S2, and S3). Miller indices are indexed at the top of peaks in Fig. 1 for each sample. The peaks appeared in the XRD pattern of as-synthesized sample S1 can be assigned to Co_3O_4 with cubic structure (JCPDS

Card No. 01-080-1536). By performing the annealing process, the crystal structure of sample S1 is accompanied with a decrease in the oxide formation, leading to an increase in the formation of metallic Co NPs (JCPDS Card No. 00-015-0806) together with $Co_3(BO_3)_2$ compound (JCPDS Card No. 01-075-1808).

In the case of sample S2, the peaks appeared in the XRD pattern of as-synthesized NPs prepared in the presence of graphite are related to *hcp*-Co and hexagonal carbon structures with (002) preferred orientation (JCPDS Card Nos. 00-005-0727 and 00-025-0284). By annealing sample S2, the Co crystal structure changes to *fcc* with (111) preferred orientation, whereas the carbon structure remains hexagonal (JCPDS Card Nos. 00-015-0806 and 00-008-0415). The XRD patterns of as-synthesized and annealed sample S3 show the same crystal structure (*fcc*) with (111) preferred orientation for Co NPs prepared in the presence of activated carbon. However, the crystallite size of sample S3 increases significantly after annealing, and the clearly defined peaks obtained for both Co and C are nearly identical to those existing prior to the heat treatment.

The intensity of Co (002) and C (002) peaks in sample S2 before annealing can be used for calculating the fraction (F) of C crystallites based on the following relation:

$$F = I_{hexagonal}/I_{total} \qquad (1)$$

where $I_{hexagonal}$ is the intensity of I_{002} of hexagonal C phase, and I_{total} is the sum of the intensities of I_{002} for both Co and C. In this way, the fraction of hexagonal C phase present in Co NPs calculated from Eq. (1) is found to be 28% [18].

The average crystallite size (D) of each sample was calculated using Scherrer formula [19] as follows:

$$D = \frac{K\lambda}{\beta \cos\theta} \qquad (2)$$

where K is the Scherrer constant, λ is the wavelength of X-rays, β is the full width at half maximum (FWHM) of the diffracted peak, and θ is the diffraction angle. The results obtained are shown in Table 1.

Table 1: The average crystallite size of Co NP samples calculated by the Scherrer equation using XRD results.

Sample	Crystallite size before annealing (nm)	Crystallite size after annealing (nm)
S1	33.54	35.11
S2	18.24	30.37
S3	18.68	36.12

FE-SEM was employed to investigate structure, surface morphology, particle size, and particle shape. Figs. 3 and 4 depict FE-SEM images of as-synthesized and annealed Co NP samples (S1, S2, and S3) along with the corresponding particle size distribution histograms, respectively. The main feature of all samples after annealing is the modification of shape and increased size of the grains (see Fig. 4). The statistical calculations of mean and standard deviation from the particle size distribution histograms

(the insets in Figs. 3 and 4) are presented in Table 2. The average crystallite sizes presented in Table 1 are in good agreement with the particle sizes determined using FE-SEM images.

Table 2: Statistical parameters of Co NP sizes extracted using FE-SEM images.

As-synthesized Co NPs					Annealed Co NPs				
Sample	**S. D.**	**Mean**	**Min**	**Max**	**Sample**	**S. D.**	**Mean**	**Min**	**Max**
S1	13.44	47.44	27.36	81.09	S1	63.17	140.60	69.61	299.82
S2	9.12	39.07	22.99	61.74	S2	9.01	45.80	26.20	65.64
S3	8.32	27.79	15.43	49.00	S3	22.33	118.72	67.62	177.13

EDX analysis was performed to verify the presence of cobalt, carbon and oxides, while also examining the binding energies and chemical compositions of the three Co NP samples [20]. The EDX spectra are presented in Fig. 2, indicating the characteristic signals for the elements cobalt (Co), oxygen (O), and carbon (C). In general, the weight percentages of cobalt, oxygen and carbon were determined from EDX spectra of as-synthesized and annealed Co NP samples (S1, S2, and S3), which can be seen as insets in Fig. 2. While the peaks at binding energies of 0.78, 6.92 and 7.68 keV correspond to CoL, $CoK\alpha$ and $CoK\beta$ radiations, respectively, the peaks at binding energies of 0.512 and 0.25 keV represent oxygen $(O-K\alpha)$ and $(C-K\alpha)$ radiations [21]. This finding confirms that sample S1 consists of cobalt oxides without carbon. Binding energies of samples S2 and S3 confirm the existence of carbonaceous cobalt compounds with no pronounced peak related to oxygen for sample S2. However, the amount of oxygen in sample S3 is less than that in sample S1. Based on the EDX spectra shown in Fig. 2, by-products exist for the synthesized Co NPs due to residuals of unreacted precursors. On the other hand, EDX spectra of annealed Co NP samples show no oxygen peaks, indicating the diminishment or significant decrease in the oxide formation. In turn, the oxide removal may play a key role in magnetic characteristics of the resulting Co NPs.

Prior to the heat treatment, magnetic characteristics of the NPs were evaluated at room temperature with a maximum applied field of 10 kOe, as depicted in Fig. 5. Table 3 presents M_s, M_r, H_c, and M_r/M_s values extracted from the hysteresis loop measurements of as-synthesized and annealed Co NPs. Despite the fact that the as-synthesized samples contain carbon and oxygen, the acquired magnetic parameters are found to be relatively high. For example, M_s values of as-synthesized samples S2 and S3 are measured to be 63.89 and 65.01 emu/g, respectively. As well, the corresponding H_c values are obtained to be 221 and 400 Oe. These magnetic characteristics outperform or are comparable to other reports in previous studies. Notably, Yang et al. [22] reported the synthesis of pure Co NPs with an average size of 16 nm using oleylamine, oleic acid and sodium oleate as surfactants, achieving M_s and H_c of 56.55 emu/g and 297.62 Oe, respectively. In another study, Yan et al. [23] prepared Co NPs (10-30 nm in size) in a graphitic shell using a

chemical vapor deposition method, obtaining M_s and H_c of 71.7 emu/g and 486 Oe, respectively. Basically, the sum of NPs has a moment of $N\mu$, where N is the number of atoms and μ is the moment per cobalt atom. In general, the heat treatment in the present study makes a noticeable impact on the magnetic parameters, particularly enhancing M_s values (see Table 3). In this case, the reduction of cobalt oxide NPs following the heat treatment causes a remarkable four-fold increase in M_s of sample S1 (from 5.59 to 20.24 emu/g). Due to the presence of graphite and activated carbon, samples S2 and S3 behave differently after annealing. The M_s of sample S2 increases from 63.89 to 99.68 emu/g, whereas sample S3 demonstrates a considerably smaller increase in M_s. This can be brought about by a number of mechanisms, including the reduction of oxides, enhanced crystallinity, and the long-range arrangement of magnetic moments following the heating treatment. In ambient temperature, stabilizing the magnetic order in conventional ferromagnetic particles, especially Co NPs, is complicated. The composition of the prepared structures reasonably reflects their magnetic behavior. Moreover, the role of carbon is obvious in preventing the formation of Co and Co_3O_4 phases in samples S2 and S3, as shown in the XRD patterns. The NPs formed based on cobalt and its oxide (Co_3O_4) play a role in the reduction of the M_s of sample S1 to 5.59 emu/g [24].

Furthermore, Co and Co_3O_4 NPs can determine the anisotropic structure of NP assembly through symmetry braking at the interface, as well as the proximity effect and potential super-exchange coupling mechanisms that result in the enhanced H_c. The presence of boron element from the reducing agent ($NaBH_4$) might contribute to the magnetic anisotropy of Co [25]. However, the amount of boron present in each sample is approximately the same, according to the EDX spectra shown in Fig. 2.

In addition to the composition, shape and size, the microstructure of the sample has a significant impact on the magnetic response. These features can be affected by the preparation methods [26,27]. The size reduction causes the magnetic anisotropy to decline, resulting in superparamagnetic relaxations at nanoscopic level of few nanometers. In these sizes, the fundamental mechanism behind the soft magnetic behavior is that, for grain sizes smaller than the ferromagnetic exchange length, the local magnetocrystalline anisotropies randomly average out. This leads to a decrease in the H_c as grain size (d) decreases. The (d^6) dependence of H_c is identified for nanocrystalline materials (down to $d = 100\,nm$). Within the realm of large grain size, the (1/d) dependence of coercivity is dominant, involving domain wall pinning at grain boundaries. It is more commonly reported that the magnetization reversal occurs for large grain sizes and bulk magnetic materials as a result of the nucleation of relatively small reversed domains (often on inhomogeneities or defects) and the subsequent propagation of magnetic domain walls [28]. The statistical mean grain sizes of as-synthesized and annealed Co NPs obtained using FE-SEM images (see Table 2) indicate the presence of grain size dependency of H_c, In other words, H_c values of samples S2 and S3 decrease by about 64% (from 221 to 80 Oe) and 58% (from 400 to 168 Oe) due to the increase in mean NP size from 39.07 to 45.80 nm and 27.79 to 118.72 nm, respectively. It is worth noting that the further reduction in H_c of sample S2 can be attributed to the reduction of

magnetocrystalline anisotropy due to the decrease in *hcp*-Co phase percentage after annealing. The results of M-H loops demonstrate that the switching field distribution (SFD) of sample S3 is significantly lower than that of samples S1 and S2. This might be due to an increased exchange interaction triggered by size dependence and/or decreased magnetocrystalline anisotropy, thereby leading to slight optimization in the overall quality of magnetic parameters. The SFD is closely related to the size distribution of particles because different particle sizes and shapes can flip at different fields. The magnetic media with high H_c and low SFD are preferred for high-density recording and spintronic devices [29].

SFD can be calculated from the equation below:

$$SFD = \frac{\Delta H}{H_c} \qquad (3)$$

where ΔH is taken at the half maximum peak of SFD curve. Also, S* represents an important value of magnetic recording media which is given by the following equation:

$$\left.\frac{dM}{dH}\right|_{H_c} = \frac{M_r}{H_c(1-S^*)} \qquad (4)$$

where $\frac{dM}{dH}$ is the slope at H_c, and M_r is the remanence magnetization [30]. Furthermore, one can calculate the energy product of magnetic NPs using the following equation:

$$(BH)_{Max} = \frac{M_r H_c}{16\pi} \qquad (5)$$

The quantitative results calculated from the above-mentioned equations are inserted in Table 3. Among the samples, $(BH)_{Max}$ of Co NPs synthesized in the presence of activated carbon (sample S3) is larger (1242.50 GOe), making them suitable for magnetic recording media applications.

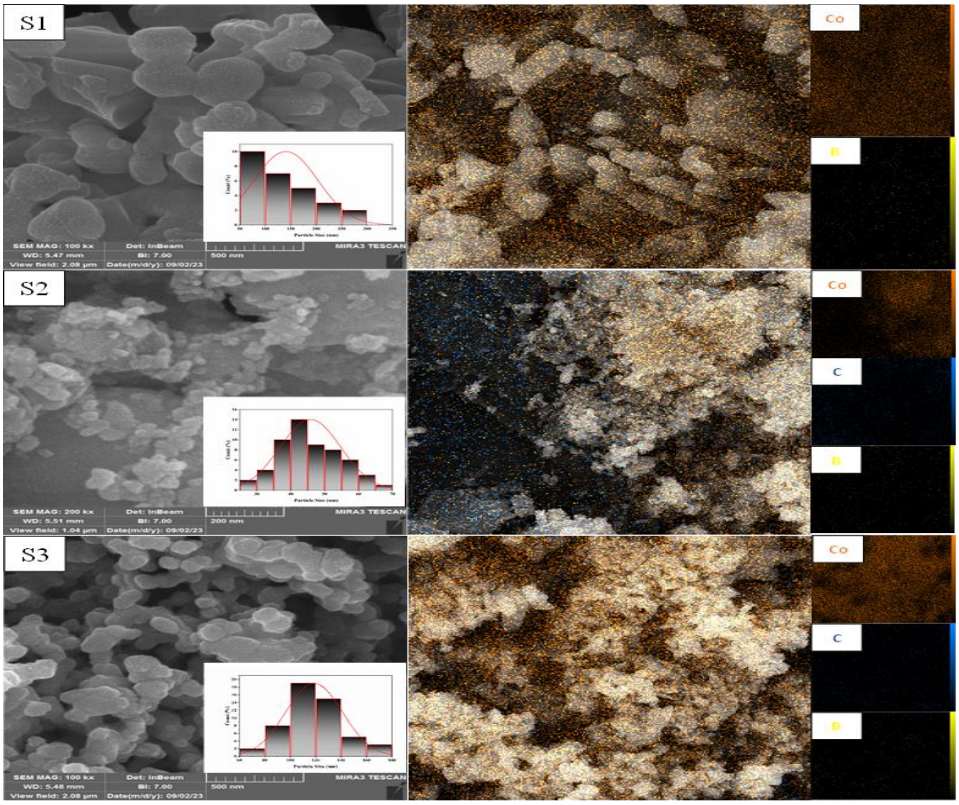

Fig. 4: FE-SEM images of annealed Co NP samples (S1, S2, and S3) (left panel). The insets represent corresponding size distribution histograms. The right panel shows EDX mapping of the samples for Co, C, and B elements recorded at the range of 2 μm.

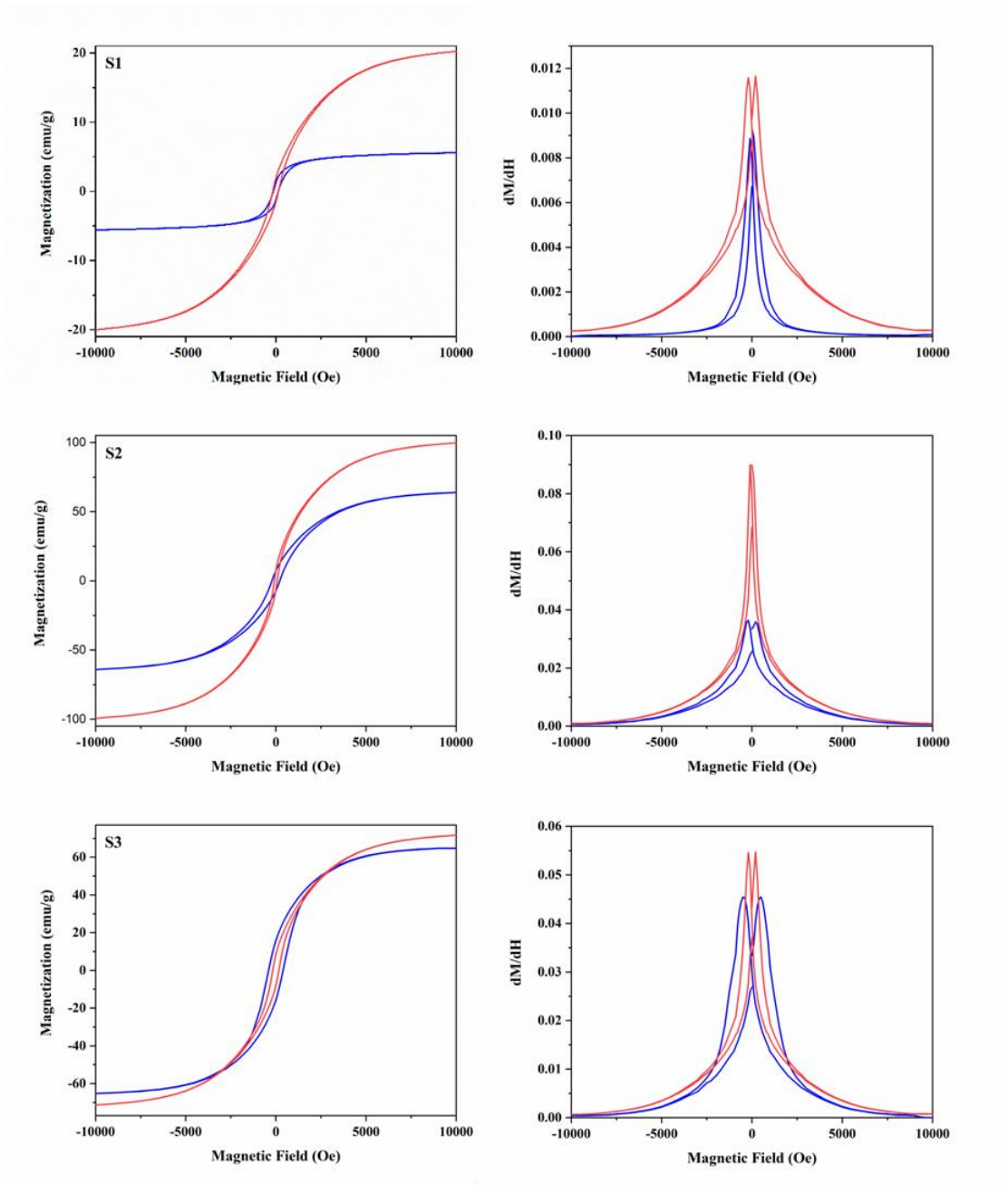

Fig. 5: Hysteresis loops of Co NP samples (S1, S2, and S3) before (blue line) and after (red line) annealing (left panel). The right panel shows the corresponding SFD curves.

Table 3: The magnetic parameters extracted from VSM hysteresis loop measurements of as-synthesized and annealed Co NP samples.

As-synthesized Co NPs							
Sample	**H_c (Oe)**	**M_r (emu/g)**	**M_s (emu/g)**	**M_r/M_s**	**$(BH)_{max}$ (GOe)**	**SFD**	**S***
S1	137	1.26	5.59	0.23	33.89	4.79	0.03
S2	221	7.35	63.89	0.12	318.94	7.75	0.39
S3	400	15.82	65.01	0.24	1242.50	4.00	0.33

Annealed Co NPs							
Sample	**H_c (Oe)**	**M_r (emu/g)**	**M_s (emu/g)**	**M_r/M_s**	**$(BH)_{max}$ (GOe)**	**SFD**	**S***
S1	80	1.90	20.24	0.09	29.85	16.33	0.64
S2	80	7.86	99.68	0.08	123.46	7.39	0.33
S3	168	8.58	71.69	0.12	283.03	5.23	0.22

5. Conclusion

In conclusion, Co and carbon-containing Co NPs were synthesized using $NaBH_4$ as a reducing agent in a one-pot chemical method, followed by performing an annealing process. The XRD patterns showed that the Co NPs were dominated by cubic Co_3O_4 crystal phase in the absence of graphite and activated carbon during the synthesis, indicating their contribution as stabilizer materials. The annealing process changed the crystal structure of Co NPs synthesized in the presence of graphite from *hcp* to *fcc*, whereas it significantly enhanced crystallite size from 18.68 to 36.12 nm for *fcc*-Co NPs synthesized in the presence of activated carbon. Meanwhile, FE-SEM images indicated the modification of morphology and enhanced mean NP sizes and distributions of annealed Co NPs. The VSM results showed relatively high M_s (up to 99.68 emu/g) values of annealed carbon-containing Co NPs. The H_c values decreased sharply after annealing, which may be caused by increased exchange interaction due to the increased NP sizes and/or decreased magnetocrystalline anisotropy of Co NPs with *fcc* crystal structure. Overall, the prepared carbon-containing Co NPs with $(BH)_{Max}$ of up to 1242.50 GOe might be suitable for magnetic device applications, including magnetic recording media.

Acknowledgements

This work was supported by University of Basrah, college of science, department of physics. The authors gratefully acknowledge the University of Basrah for providing the financial support of this work.

References

[1] B. Pelaz, C. Alexiou, R.A. Alvarez-Puebla, F. Alves, A.M. Andrews, S. Ashraf, L.P. Balogh, L. Ballerini, A. Bestetti, C. Brendel, Diverse applications of nanomedicine, ACS Nano 11 (2017) 2313–2381.

[2] H. Zeng, S. Sun, Syntheses, properties, and potential applications of multicomponent magnetic nanoparticles, Adv Funct Mater 18 (2008) 391–400.

[3] K.A. Mohammed, K.M. Ziadan, A.S. Al-Kabbi, K.K. Saxena, R.S. Zabibah, A.J. Alrubaie, J.H. Mohammed, Optical, morphological, electrical properties and white light photoresponse of CdSe nanoparticles, Advances in Materials and Processing Technologies 8 (2022) 2289–2298. https://doi.org/10.1080/2374068X.2022.2037877.

[4] G. Salazar-Alvarez, J. Qin, V. Sepelak, I. Bergmann, M. Vasilakaki, K.N. Trohidou, J.D. Ardisson, W.A.A. Macedo, M. Mikhaylova, M. Muhammed, Cubic versus spherical magnetic nanoparticles: the role of surface anisotropy, J Am Chem Soc 130 (2008) 13234–13239.

[5] Q. Yuanchun, Z. Yanbao, W. Zhishen, Preparation of cobalt oxide nanoparticles and cobalt powders by solvothermal process and their characterization, Mater Chem Phys 110 (2008) 457–462. https://doi.org/10.1016/j.matchemphys.2008.03.001.

[6] H. Tian, X. Li, L. Zeng, J. Gong, Recent advances on the design of group VIII base-metal catalysts with encapsulated structures, ACS Catal 5 (2015) 4959–4977.

[7] W.J. Tseng, C.-N. Chen, Dispersion and rheology of nickel nanoparticle inks, J Mater Sci 41 (2006) 1213–1219.

[8] J.H. Mokkath, Ultraviolet plasmon resonance in transition-metal doped aluminum nanoparticle arrays, J Mater Chem C Mater 6 (2018) 2225–2228.

[9] M.A. Hines, P. Guyot-Sionnest, Synthesis and characterization of strongly luminescing ZnS-capped CdSe nanocrystals, J Phys Chem 100 (1996) 468–471.

[10] R.C. Ashoori, Electrons in artificial atoms, Nature 379 (1996) 413–419.

[11] T. Hayashi, T. Ohno, S. Yatsuya, R. Uyeda, Formation of ultrafine metal particles by gas-evaporation technique. IV. Crystal habits of iron and Fcc metals, Al, Co, Ni, Cu, Pd, Ag, In, Au and Pb, Jpn J Appl Phys 16 (1977) 705.

[12] Y.W. Zhao, R.K. Zheng, X.X. Zhang, J.Q. Xiao, A Simple Method to Prepare Uniform Co Nanoparticles, IEEE Trans Magn 39 (2003) 2764–2766. https://doi.org/10.1109/TMAG.2003.815592.

[13] R.M. de Silva, V. Palshin, K.M.N. de Silva, L.L. Henry, C.S.S.R. Kumar, A new role for surfactants in the formation of cobalt nanoparticles, J Mater Chem 18 (2008) 738–747.

[14] Y. Chen, K.Y. Liew, J. Li, Size controlled synthesis of Co nanoparticles by combination of organic solvent and surfactant, Appl Surf Sci 255 (2009) 4039–4044.

[15] B. Morcos, P. Lecante, R. Morel, P.-H. Haumesser, C.C. Santini, Magnetic, structural, and chemical properties of cobalt nanoparticles synthesized in ionic liquids, Langmuir 34 (2018) 7086–7095.

[16] A. Kotoulas, C. Dendrinou-Samara, C. Sarafidis, T. Kehagias, J. Arvanitidis, G. Vourlias, M. Angelakeris, O. Kalogirou, Carbon-encapsulated cobalt nanoparticles: synthesis, properties, and magnetic particle hyperthermia efficiency, Journal of Nanoparticle Research 19 (2017) 1–14.

[17] S.M. Saleh Al-Khazali, H.S. Al-Salman, A. Hmood, Low cost flexible ultraviolet photodetector based on ZnO nanorods prepared

using chemical bath deposition, Mater Lett 277 (2020). https://doi.org/10.1016/j.matlet.2020.128177.

[18] G.M. Al-Senani, N.M. Deraz, O.H. Abd-Elkader, Magnetic and characterization studies of CoO/Co3O4 nanocomposite, Processes 8 (2020) 844.

[19] N.A. Abdullah, B. Ali, H. Jabbar, Study the Effect of Tio2 Nanoparticles in Multilayers of Photoelectrode Prepared by Ball Milling Technique on the Performance of Dye Sensitized Solar Cells (Dsscs), in: J Phys Conf Ser, IOP Publishing Ltd, 2021. https://doi.org/10.1088/1742-6596/1818/1/012069.

[20] A. Ahmed S. Abed, S. J. Kasim, A. F. Abbas, Optical and Structural Properties of CdS Quantum Dots Synthesized Using (MW-CBD) Technique, Iraqi Journal of Nanotechnology (2020) 44–52. https://doi.org/10.47758/ijn.vi1.29.

[21] Zainab K. Ali, Mazin A. Mahdi, Preparation of Silicon Nanowires Photocathode for Photoelectrochemical Water Splitting, Iraqi Journal of Physics 20 (2022) 66–81. https://doi.org/10.30723/ijp.v20i4.1070.

[22] X. Yang, H.P. Shao, Synthesis and Characterization of Cobalt Nanoparticles by Cobalt-Acetate, Adv Mat Res 503 (2012) 346–349.

[23] J. Yan, T. Wei, J. Feng, Z. Fan, L. Zhang, F. Wei, One step synthesis of nanoparticles of cobalt in a graphitic shell anchored on graphene sheets, Carbon N Y 50 (2012) 2356–2358.

[24] A.S. Lozhkomoev, A. V Pervikov, S.O. Kazantsev, K. V Suliz, R. V Veselovskiy, A.A. Miller, M.I. Lerner, Controlled oxidation of cobalt nanoparticles to obtain Co/CoO/Co3O4 composites with different Co content, Nanomaterials 12 (2022) 2523.

[25] E. Meydan, S. Demirci, N. Aktas, N. Sahiner, O.F. Ozturk, Boron-containing magnetic nanoparticles from Co, Ni, and Fe chloride salts and their catalytic performances on 4-nitrophenol reduction, Inorg Chem Commun 116 (2020) 107930.

[26] R. Hasegawa, Design and fabrication of new soft magnetic materials, J Non Cryst Solids 329 (2003) 1–7.

[27] G. Herzer, Soft magnetic nanocrystalline materials, Scripta Metallurgica et Materialia 33 (1995) 1741–1756.

[28] J. Vogel, J. Moritz, O. Fruchart, Nucleation of magnetisation reversal, from nanoparticles to bulk materials, C R Phys 7 (2006) 977–987.

[29] J.C. Mallinson, The foundations of magnetic recording, Elsevier, 2012.

[30] F. Kalil, A. Buschman, HIGH-DENSITY DIGITAL RECORDING., NASA Reference Publication (1985). https://doi.org/10.1007/978-94-011-1636-7.